

Article

Free Vibration Analysis of Functionally Graded Sandwich Plates with a Homogeneous Core

J.R. Cho 

Department of Naval Architecture and Ocean Engineering, Hongik University, Jochiwon, Sejong 30016, Korea; jrcho@hongik.ac.kr; Tel.: +82-44-860-2546

Featured Application: Novel design of functionally graded metal-ceramic sandwich plates.

Abstract: The functionally graded (FG) sandwich plate has attained much attention in recent years due to its potential for exhibiting the merits of sandwich construction and FGM. Accordingly, intensive studies have focused on FG sandwich plates to investigate their mechanical behaviors. However, these mechanical behaviors are still in need of further investigation, particularly with respect to the major parameters. In this context, this paper intends to parametrically investigate the free-vibration behavior of the FG sandwich plate with a homogeneous core by developing a reliable and effective numerical method. This numerical method was based on hierarchical models, developed from the spectral model accuracy, and the 2-D natural element method (NEM). The hierarchical models were derived from the 3-D elasticity and the NEM was characterized by high smooth interpolation functions. From the verification experiments, the proposed method shows a good agreement with the reference and a uniform convergence to the 3-D elasticity. The free vibration characteristics of FG sandwich plates with a homogeneous core were investigated using the proposed numerical method. It was found that the calibrated fundamental frequency was significantly influenced by the type of material composing the core, the volume fraction index, the relative thickness and position of core layer, and the plate aspect ratio.

Keywords: functionally graded sandwich plate; homogeneous core; FGM face; free vibration analysis; hierarchical models; natural element method



Citation: Cho, J. Free Vibration Analysis of Functionally Graded Sandwich Plates with a Homogeneous Core. *Appl. Sci.* **2022**, *12*, 6054. <https://doi.org/10.3390/app12126054>

Academic Editor: Francesco Tornabene

Received: 30 May 2022

Accepted: 13 June 2022

Published: 14 June 2022

Publisher's Note: MDPI stays neutral with regard to jurisdictional claims in published maps and institutional affiliations.



Copyright: © 2022 by the author. Licensee MDPI, Basel, Switzerland. This article is an open access article distributed under the terms and conditions of the Creative Commons Attribution (CC BY) license (<https://creativecommons.org/licenses/by/4.0/>).

1. Introduction

Conventional sandwich structures are characterized by a functional lamination construction of homogeneous layers. A representative example is a three-layered sandwich plate, which is composed of two thin, stiff face sheets and a relatively thick, lightweight core. Both the faces and core are firmly bonded to ensure the load transfer between constituent layers. Combining the superior performance qualities of each laminate, they have been broadly accepted in various engineering applications. For example, the high strength-to-weight ratio of sandwich structures greatly advanced composite-associated industries over several decades, particularly the transportation industry. However, conventional sandwich structures suffer from a major defect: the abrupt change in material properties across the lamina interfaces [1]. This inherent mismatch of material properties may degrade the target performance of the sandwich and even induce microcracking, which results in delamination. In order to resolve this problem, the concept of functionally graded materials, which was introduced by a group of Japanese scientists in 1980s [2], was extended to sandwich structures [3].

The concept of FGM was originally intended to minimize the thermal stress concentration at the interface of the conventional, bi-material-type, heat-resisting composites by inserting a graded layer. The graded layer is manufactured by mixing two constituent particles such that the volume fraction of one particle varies continuously from 100% at

one side to 0% at the other side. Therefore, the conventional mismatch problem does not occur any longer; it is prevented through the insertion of a graded layer between two base homogeneous layers. Furthermore, the target performance of FGM could be maximized by optimally tailoring the thickness-wise distribution of volume fraction [4,5]. Due to these excellent properties, the notion of FGM has received the considerable attention in various engineering fields. In heat-resisting FGMs, the two base materials are generally metal and ceramic, and this combination has been also adopted for other engineering applications [6]. Here, the FGM plates with this construction are known as a functionally graded sandwich plate with homogeneous faces and a FGM core [7,8]. As a straightforward extension of three-layered metal-ceramic FGMs, this type of FG sandwich plate has been widely investigated. Another type is the functionally graded sandwich plate with FGM faces and a homogeneous core [9–11]. This type is, once again, divided into softcore and hardcore, based on whether the material composing the core is metal or ceramic.

The FG sandwich structures have attained considerable attraction for their novel design of engineering structures, because they have a potential for exhibiting all the advantages of sandwich construction and FGM. Accordingly, extensive studies have been progressed to investigate the major mechanical behaviors of FG sandwich structures. In early studies, the bending, vibration, and buckling responses were analytically analyzed using the first-order shear deformation plate theory (FSDT) [3,12,13]. Later, a new refined plate theory for the simply supported FG sandwich plate was proposed by subsequent investigators [14–16]. Meanwhile, numerical studies using the refined finite element methods [9,17] and a layerwise finite element approximation [18] have been also reported. Furthermore, a meshless method was introduced for the numerical investigation of free vibration of FG sandwich plates [19].

More recently, Bennoun et al. [10] proposed a five-variable, refined plate theory for the accurate and effective vibration analysis of FG sandwich plates. Di Sciuva and Sorrenti [20] assessed the performance of the refined zigzag theory to the analysis of bending and free vibration of FG sandwich plates. Liu et al. [21] semi-analytically investigated the free vibration of FG sandwich plates through the scaled boundary element method, in which a layerwise approach based on 3D elasticity theory was adopted. Vinh [22,23] investigated the static bending, free vibration and buckling of a bi-directional FG sandwich plate through a hybrid, quasi-3D theory and the combination of a higher-order, shear deformation theory with FEM. Vinh and Huy [24] established the FE model, based on a new hyperbolic SDT, to investigate the static bending, free vibration and buckling of FG sandwich plates with porosity. Hirane et al. [25] presented a novel C^0 higher-order layerwise FE model for the static and free vibration analysis of FG sandwich plates in which the number of variables does not increase when increasing the number of layers. Belarbi et al. [26] studied the size-dependent, free vibration response of FG nanoplates using a layerwise theory, and Vinh and Tounsi [27] investigated the role of spatial variation of the nonlocal parameter on the free vibration of FG sandwich nanoplates.

However, the free-vibration behavior of the FG sandwich plate is still in need of parametric investigation with respect to the major parameters such as the aspect ratio. Moreover, the NEM has been mostly applied to non-sandwich plate-like structures, such that its application to FG sandwich plates has been rarely reported. Therefore, the parametric free vibration investigation of the FG sandwich plate through the NEM has significance. In this context, this paper intends to introduce a reliable and effective numerical method for investigating the free vibration characteristics of FG sandwich plates with homogeneous cores. The numerical method was based upon hierarchical models showing the spectral modeling error and implemented by the 2-D natural element method (NEM) [28,29]. The hierarchical models were derived from 3-D elasticity and the NEM is a type of meshfree method characterized by smooth Laplace interpolation functions [30]. The proposed method was verified by comparing it with the reference and 3-D elasticity. Using the developed method, the free vibration characteristics of FG sandwich plates with homogeneous cores were

parametrically investigated with respect to the material type of core, the volume fraction index, and the relative thickness and position of core.

2. FG Sandwich Plates with Homogeneous Cores

Figure 1 represents a general rectangular FG sandwich plate composed of three layers, in which three layers are macroscopically homogeneous or inhomogeneous. The lengths of the two sides are a and b , and the uniform thickness of plate is denoted by h . A Cartesian coordinate system (x, y, z) is positioned at the center, on the mid-surface of the plate such that the top and bottom surfaces of the plate are located at $z = \pm h/2$ in the z -direction. The plate could be non-symmetric with respect to the material property and/or the geometric dimension. The three layers are numbered as *Layer 1*, *Layer 2*, and *Layer 3* from the bottom to the top of the plate, and the thickness-wise intervals of each layer are set by $(I = 1, 2, 3)$.

$$\text{Layer } I, z \in [h_I, h_{I+1}] \tag{1}$$

Meanwhile, for the convenience of notation, the *pseudo-thickness ratio* of each layer from the bottom to the top is denoted by $H_1 - H_2 - H_3$ ($H_I = 0, 1, 2, \dots$) in terms of three numbers H_I . Then, the actual thickness ratios $R_I \in [0, 1]$ of each layer were calculated as following:

$$R_I = \frac{H_I}{H_1 + H_2 + H_3} \tag{2}$$

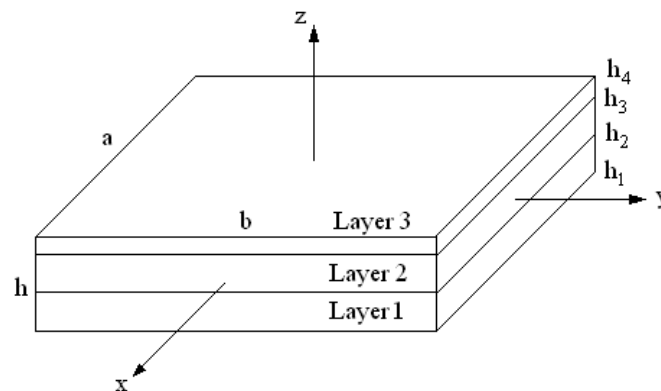


Figure 1. Geometry and dimensions of a non-symmetric, rectangular FG sandwich plate with uniform thickness.

FG sandwich plates are classified into two types, one with FGM face sheets and a homogeneous core (*Type A*) and the other with homogeneous face sheets and an FGM core (*Type B*). In the current study, Type A is shown in Figure 2, where the white and black layers are homogeneous, while the layers with gray spectrum are FGM. In the figure, the plot indicates the volume fraction distributions, where power-law functions are adopted for FGM face sheets in Type A. Let us denote $V(z) \in [0, 1]$ and $\tilde{V}(z) \in [0, 1]$ as two volume fractions which obey the following physical constraint, given by:

$$V(z) + \tilde{V}(z) = 1.0, \quad z \in [-h/2, h/2] \tag{3}$$

In the current study, the core material was calculated through $V(z)$, as represented in Figure 2.

Due to the physical constraints, either one of the two volume fractions was sufficient to identify the volume fraction distributions of the FG sandwich plate. The volume fraction, $V(z)$, was calculated for the current study, then expressed by a linear combination of layer-wise continuous volume fractions, $V^{(I)}(z)$, such that

$$V(z) = V^{(1)}(z) + V^{(2)}(z) + V^{(3)}(z) \tag{4}$$

where $V^{(l)}(z)$ are defined by

$$V^{(1)} = \left(\frac{z - h_1}{h_2 - h_1} \right)^n, z \in [h_1, h_2] \tag{5}$$

$$V^{(2)} = 1, z \in [h_2, h_3] \tag{6}$$

$$V^{(3)} = \left(\frac{z - h_3}{h_4 - h_3} \right)^n, z \in [h_3, h_4] \tag{7}$$

Here, the core material could be metal or ceramic, where the former case is described as *softcore* while the latter is described as *hardcore*. In other words, $V(z)$ indicates the metal volume fraction for softcore cases and the ceramic volume fraction for hardcore cases.

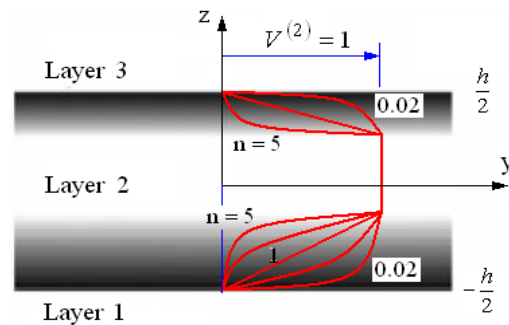


Figure 2. Volume fraction distributions through the thickness of an FG sandwich plate with two FGM facesheets and a homogeneous core (Type A).

Next, the effective material properties $\bar{M}_{eff}(z)$ at any point within of FG sandwich plate were evaluated as

$$\bar{M}_{eff}(z) = V(z)M + [1 - V(z)]\tilde{M} \tag{8}$$

according to the linear rule of mixtures [31]. M and \tilde{M} indicate the properties of the metal and the ceramic cases, respectively. The variation of $\bar{M}_{eff}(z)$ through the thickness was reflected in the process of numerical integration of mass and stiff matrices in natural element approximation, as explained in the next section.

3. Natural Element Free Vibration Approximation

Viewing the FG sandwich plate as a 3-D, linearly elastic body, its harmonic motion was denoted by $\underline{u}(x; t) = \underline{u}(x)e^{j\omega t}$. Then, the free vibration of FG sandwich plate was determined to be governed by $(\alpha, \beta = x, y, z)$

$$\sigma_{\alpha\beta} \left(\underline{u} \right)_{,\beta} = \omega^2 \rho \bar{u}_\alpha \text{ in } \varpi \times [-h/2, h/2] \tag{9}$$

with the displacement boundary condition:

$$\underline{u} = \hat{\underline{u}} \text{ on } \partial\varpi_D \times [-h/2, h/2] \tag{10}$$

where, $\sigma_{\alpha\beta}$ and ρ are Cauchy stresses and the effective density, and ϖ and $\partial\varpi_D$ indicate the plate mid-surface and the displacement boundary region, respectively.

Meanwhile, in the (q_x, q_y, q_z) hierarchical model, the triple-vector amplitude function, $\underline{u}(x)$, is expressed as [28]

$$\bar{u}_\alpha(x) = \sum_{\ell=0}^{q_\alpha} \bar{U}_\alpha^\ell(x, y) \cdot \left(\frac{2z}{h} \right)^\ell \tag{11}$$

where, $\bar{U}_\alpha^\ell(x, y)$ are in-plane amplitude functions defined on the plate’s mid-surface, which were determined through the 2-D natural element method. For the natural approximation, the mid-surface of the sandwich plate was discretized by N grid points (i.e., nodes) and N_D Delaunay triangles. This construction of grid points and Delaunay triangles was generated by an NEM grid, as shown in Figure 3a. To each grid point J , Laplace interpolation functions, $\phi_J(x)$, shown in Figure 3b, were assigned. The definition and characteristics of these functions may be found at the following references: [32,33]. Using these interpolation functions, both the trial and test functions, $\mathbf{u}^{-q,h}$ and $\mathbf{v}^{q,h}$, were approximated as

$$\bar{u}_\alpha^{-q,h}(\mathbf{x}) = \sum_{J=1}^N \bar{U}_{\alpha,J}^0 \phi_J(x, y) \cdot \left(\frac{2z}{d}\right)^0 + \dots = \sum_{m=0}^{q_\alpha} \left(\sum_{J=1}^N \bar{U}_{\alpha,J}^m \phi_J(x, y) \right) \cdot \left(\frac{2z}{d}\right)^m \quad (12)$$

$$v_\beta^{q,h}(\mathbf{x}) = \sum_{I=1}^N V_{\beta,I}^0 \phi_I(x, y) \cdot \left(\frac{2z}{d}\right)^0 + \dots = \sum_{\ell=0}^{q_\beta} \left(\sum_{I=1}^N V_{\beta,I}^\ell \phi_I(x, y) \right) \cdot \left(\frac{2z}{d}\right)^\ell \quad (13)$$

Assuming that $q_x = q_y = q_z = q$ for the concise expression purpose, the virtual strain vector $\boldsymbol{\varepsilon}(\mathbf{v}^{-q,h})$ and the actual stress vector $\boldsymbol{\sigma}(\mathbf{u}^{-q,h})$ were expressed by

$$\boldsymbol{\varepsilon}(\mathbf{v}^{-q,h}) = \sum_{\ell=0}^q \sum_{I=1}^N \mathbf{L} \phi_I \bar{V}_I^\ell \cdot \left(\frac{2z}{d}\right)^\ell = \sum_{\ell=0}^q \sum_{I=1}^N \mathbf{B}_I^m \bar{V}_I \cdot \left(\frac{2z}{d}\right)^\ell \quad (14)$$

$$\boldsymbol{\sigma}(\mathbf{u}^{-q,h}) = \mathbf{E} \boldsymbol{\varepsilon}(\mathbf{u}^{-q,h}) = \sum_{m=0}^q \sum_{J=1}^N \mathbf{B}_J^m \mathbf{U}_J^m \cdot \left(\frac{2z}{d}\right)^m \quad (15)$$

in which the matrix \mathbf{B}_J^m , containing partial differential operators, is defined by

$$\mathbf{B}_J^m = \begin{bmatrix} \partial \phi_J / \partial x & 0 & 0 & \partial \phi_J / \partial y & 0 & m \phi_J / z \\ 0 & \partial \phi_J / \partial y & 0 & \partial \phi_J / \partial x & m \phi_J / z & 0 \\ 0 & 0 & m \phi_J / z & 0 & \partial \phi_J / \partial y & \partial \phi_J / \partial x \end{bmatrix}^T \quad (16)$$

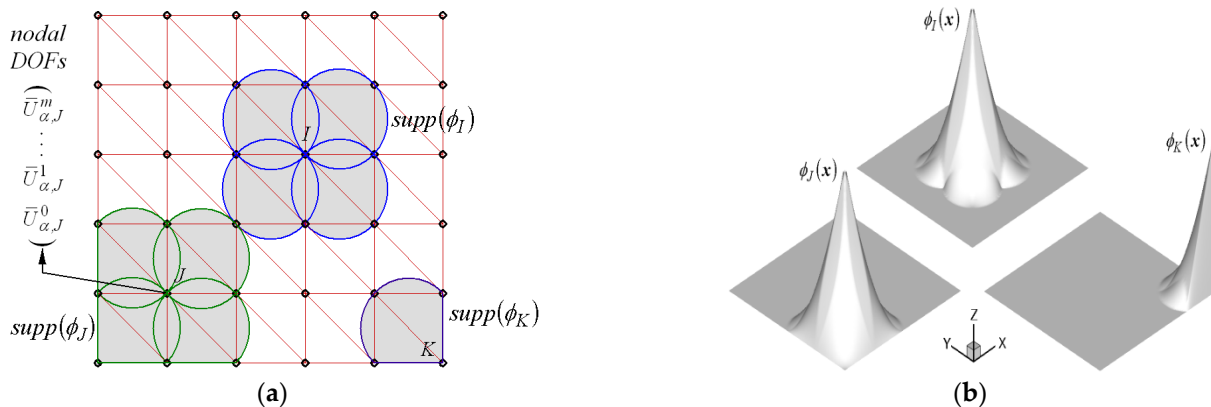


Figure 3. Natural element method: (a) NEM grid, (b) Laplace interpolation functions.

Then, substituting Equations (12)–(15) into the variational form [29] of the free vibration problem (9) generated the linear modal equation

$$(\mathbf{K} - \omega^2 \mathbf{M}) \bar{\mathbf{U}} = 0 \quad (17)$$

for computing the natural frequencies $\{\omega_i\}_{i=1}^N$ and the natural modes $\{\mathbf{U}_i\}_{i=1}^N$. Here, the stiffness and mass matrices are defined by

$$[\mathbf{K}]_{\alpha\beta, IJ}^{\ell m} = \int_{-h/2}^{h/2} \left[\int_{\omega} \left\{ (\mathbf{B}_I^T \mathbf{E}_1 \mathbf{B}_J) + (\mathbf{B}_I^T \mathbf{E}_2 \mathbf{B}_J)_{RI} \right\} d\omega \right] \cdot \left(\frac{2z}{h} \right)^{\ell+m} dz \quad (18)$$

$$[\mathbf{M}]_{\alpha\beta, IJ}^{\ell m} = \int_{-h/2}^{h/2} \left[\int_{\omega} \rho(\phi_I \mathbf{I})(\phi_J \mathbf{I}) d\omega \right] \cdot \left(\frac{2z}{h} \right)^{\ell+m} dz \quad (19)$$

with \mathbf{I} being the (3×3) identity matrix. The subscript RI indicates the selectively reduced integration (SRI) [34], using one Gaussian point, to suppress shear locking for the bending-dominated, thin structures. In order to employ the reduced integration, the material matrix \mathbf{E} was divided as follows:

$$\mathbf{E}_1 = \begin{bmatrix} E_1 & E_2 & E_2 & 0 & 0 & 0 \\ E_2 & E_1 & E_2 & 0 & 0 & 0 \\ E_2 & E_2 & E_1 & 0 & 0 & 0 \\ 0 & 0 & 0 & G & 0 & 0 \\ 0 & 0 & 0 & 0 & 0 & 0 \\ 0 & 0 & 0 & 0 & 0 & 0 \end{bmatrix}, \quad \mathbf{E}_2 = \text{diag}(0, 0, 0, 0, G', G') \quad (20)$$

with

$$E_1 = \frac{(1-\nu)E}{(1-2\nu)(1+\nu)} \text{ when } q_z \geq 1, \quad E_1 = \frac{E}{(1-\nu^2)} \text{ when } q_z = 0 \quad (21)$$

and $E_2 = \nu E_1$, $G = E/2(1+\nu)$ and $G' = G/\kappa$, where κ is the modified shear correction factor (MSCF) calculated by $\kappa = \max(1.2, 1 + C \cdot A_{mid}/h^2)$ with A_{mid} is the area of each Delaunay triangle. The generic constant C was determined through the preliminary experiment for verifying the proposed numerical method.

4. Numerical Results

4.1. Verification

A simply supported, rectangular FG sandwich plate, shown in Figure 4a, was taken to verify the proposed numerical method, where the lengths of the two sides, a and b , were 1.0m and the thickness h was taken as variable. The two constituent materials were Al and Al_2O_3 , and their mechanical properties are given in Table 1. The metallic Al was used for the softcore while the ceramic Al_2O_3 was used for the hardcore, respectively. To numerically implement the (q_x, q_y, q_z) hierarchical model, the mid-surface of the sandwich plate was uniformly discretized by an 11×11 set of grid points, as shown in Figure 4b.

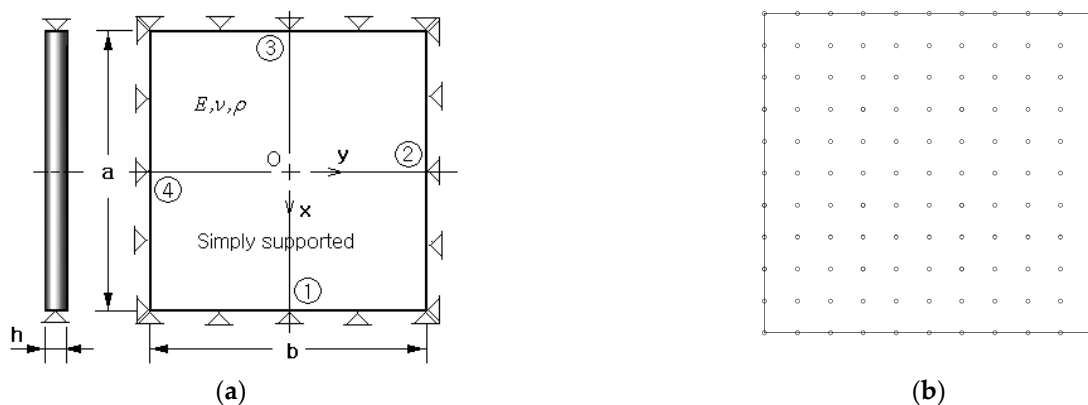


Figure 4. A simply supported, rectangular FG sandwich plate: (a) the geometric dimensions and loading/boundary conditions, (b) an 11×11 uniform NEM grid.

Table 1. Material properties of metallic and ceramic constituents.

Constituents		Young's Modulus E (GPa)	Poisson's Ratio ν	Density ρ (kg/m ³)
Metal	$A\ell$	70	0.3	2707
Ceramic	$A\ell_2O_3$	380	0.3	3800

The simply supported constraint was implemented as follows: $\bar{U}_z^0 = 0$ for all four sides of the mid-surface, $\bar{U}_x^0 = \dots = \bar{U}_x^{q_x} = 0$ for the two sides labelled ① and ③, and $\bar{U}_y^0 = \dots = \bar{U}_y^{q_y} = 0$ for the other two sides, ② and ④. The stiffness and mass matrices in Equations (18) and (19) were computed by combining the 2-D, in-plane Gaussian integration rule (7 points) and the thickness-wise trapezoidal rule (30 uniform segments). The lowest nine natural frequencies and natural modes were solved through the Lanczos transformation method and the Jacobi iteration method.

The fundamental frequencies, $\omega_{(1,1)}$, of the (2-2-1) FG sandwich plates with softcores (i.e., Ni cores) were computed using the hierarchical models and calibrated according to

$$\bar{\omega} = \frac{\omega b^2}{h} \sqrt{\frac{\rho_0}{E_0}} \quad (22)$$

where $\rho_0 = 1.0 \text{ kg/m}^3$ and $E_0 = 1.0 \text{ GPa}$. The numerical experiments were parametrically carried out with respect to the width-to-thickness ratio b/h for the same volume fraction index, n , of unity. The computed calibrated fundamental frequencies are given in Table 2 and represented in Figure 5, where the solutions of 3-D elasticity were obtained by ANSYS [35] using 10,000 3-D shell elements. All the hierarchical models showed the remarkable relative differences in $\bar{\omega}$ for thick plates, such that they overestimate the fundamental frequencies with non-negligible differences. However, for a specific value of b/h , the hierarchical models showed the spectral model accuracy such that their relative differences uniformly decreased, proportional to the model level, q . Furthermore, the relative differences of all the hierarchical models monotonically decreased in proportion to the width-to-thickness ratio b/h . In particular, it was observed that the relative difference became remarkably smaller when the model level equaled or exceeded (3,3,2), regardless of the width-to-thickness ratio. Meanwhile, both the (9,9,8) hierarchical model and the 3-D elasticity approach to the same limit equated to 1.6595, which was the solution provided by the classical laminated plate theory (CLPT) [36]. Meanwhile, it was observed that the limit values, $\bar{\omega}$, of other hierarchical models became slightly larger as the model level, q , decreased. However, the relative difference of the (1,1,0) model was 2.773% at $b/h = 500$; hence, the lower-order models were not expected to cause inaccuracy problems in the free vibration analysis for thin FG sandwich plates with homogeneous cores. The generic constant, C , which was involved in the modified shear correction factor (MSCF), was evaluated as 3/2 through this limit experiment.

Next, the (1,1,0) hierarchical model was compared with the five-variable, refined plate theory of Bennoun et al. [10]. The former was equivalent to the first-order shear deformation theory (FSDT) and the latter was refined from the FSDT. Table 3 presents the comparison for the (2-2-1) FG sandwich with a softcore (i.e., $A\ell$ layer). The relative error uniformly decreased in proportion to the width-to-thickness ratio, b/h , except for the volume fraction, $n = 0$, which demonstrated the reverse trend. Here, the (2-2-1) FG sandwich resembled a pure homogeneous plate of $A\ell$ when n is 0. Regarding the volume fraction, n , the largest errors occurred at $n = 1$ for $b/h = 5$, $n = 5$ for $b/h = 10$, and $n = 10$ for $b/h = 100$. Thus, the present method using the (1,1,0) hierarchical model was in good agreement with the FSDT, such that the overall relative error ranged from 0.895% to 5.843%, with a relatively coarse NEM grid.

Table 2. The model limits of the calibrated fundamental frequencies, $\bar{\omega}$, of hierarchical models for simply supported, square FG sandwich plates with homogeneous softcores (2-2-1, $n = 1$).

Hierarchical Models	Width-to-Thickness Ratio (b/h)					
	3	5	10	30	100	500
(1,1,0)	1.18979 (28.350%)	1.44776 (13.687%)	1.61397 (6.604%)	1.69192 (3.167%)	1.70425 (2.808%)	1.70550 (2.773%)
(1,1,2)	1.15453 (24.546%)	1.43293 (12.514%)	1.60610 (6.084%)	1.68401 (2.685%)	1.69614 (2.319%)	1.69736 (2.283%)
(3,3,2)	1.03051 (11.167%)	1.33049 (4.470%)	1.54583 (2.103%)	1.64808 (0.494%)	1.66357 (0.354%)	1.66513 (0.340%)
(3,3,4)	1.00808 (8.748%)	1.32349 (3.921%)	1.54501 (2.049%)	1.64804 (0.491%)	1.66355 (0.353%)	1.66510 (0.339%)
(9,9,8)	0.96431 (4.026%)	1.29846 (1.955%)	1.53366 (1.299%)	1.64174 (0.107%)	1.65786 (0.001%)	1.65948 (0.0%)
3-D elasticity	0.92699	1.27356	1.51399	1.63998	1.65770	1.65948

* The values in parentheses are the relative percentage differences with respect to 3-D elasticity.

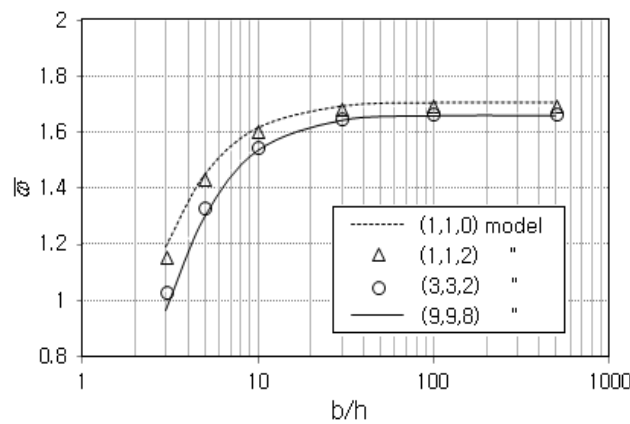


Figure 5. Variation of the calibrated fundamental frequency, $\bar{\omega}$, with respect to the width-to-thickness ratio b/h .

Table 3. Comparison of calibrated fundamental frequencies, $\bar{\omega}$, for simply supported square FG sandwich plates with homogeneous softcores (2-2-1).

b/h	Method	n				
		0	0.5	1	5	10
5	Bennoun [10]	0.85405	1.25633	1.36784	1.52684	1.55459
	Present	0.86375	1.31196	1.44776	1.61419	1.63609
	(Relative error)	(1.136%)	(4.428%)	(5.843%)	(5.721%)	(5.243%)
10	Bennoun [10]	0.92984	1.44124	1.58470	1.75986	1.78200
	Present	0.94416	1.45987	1.61397	1.79491	1.81655
	(Relative error)	(1.540%)	(1.293%)	(1.847%)	(1.993%)	(1.939%)
100	Bennoun [10]	0.96099	1.52702	1.68761	1.86908	1.88725
	Present	0.99343	1.54069	1.70425	1.89418	1.91633
	(Relative error)	(3.376%)	(0.895%)	(0.986%)	(1.343%)	(1.541%)

Table 4 presents a comparison of (2-2-1) FG sandwiches with hardcores (i.e., Al_2O_3 layers), in which the sandwich resembles a pure homogeneous plate of Al_2O_3 when n is 0. The relative error varied from 0.044% to 7.961%, so the range of relative errors was wider than in the softcore case. Contrary to the softcore, the relative error for hardcores uniformly increased in proportion to the width-to-thickness ratio, b/h , for all the volume fraction indices, n . Regarding the volume fraction index n , the largest error occurred at $n = 0$ for $b/h = 5$, and $n = 5$ for $b/h = 10$ and $b/h = 100$, which is similar to the softcore

case. From the comparison for both the softcore and hardcore cases, it has been confirmed that present method using the (1,1,0) hierarchical model showed a reasonable agreement with the five-variable, refined plate theory, with a maximum relative error equal to 7.961%. Moreover, it is expected that the accuracy of the present method would be improved when higher-order hierarchical models are used.

Table 4. Comparison of calibrated fundamental frequencies, $\bar{\omega}$, for simply supported square FG sandwich plates with homogeneous hardcores (2-2-1).

<i>b/h</i>	Method	<i>n</i>				
		0	0.5	1	5	10
5	Bennoun [10]	1.67949	1.44770	1.31762	1.06611	1.02325
	Present	1.69856	1.46343	1.32876	1.06944	1.02370
	(Relative error)	(1.135%)	(1.087%)	(0.845%)	(0.312%)	(0.044%)
10	Bennoun [10]	1.82854	1.55146	1.40103	1.11900	1.07233
	Present	1.85670	1.58688	1.43531	1.14988	1.10044
	(Relative error)	(1.540%)	(2.283%)	(2.454%)	(2.760%)	(2.621%)
100	Bennoun [10]	1.88978	1.59246	1.43337	1.13887	1.09070
	Present	1.95360	1.67033	1.51270	1.21815	1.16698
	(Relative error)	(3.377%)	(4.890%)	(5.535%)	(7.961%)	(6.994%)

4.2. Free Vibration Characteristics

Next, the free vibration characteristics of FG sandwich plates with homogeneous cores were investigated with respect to the major parameters of the plates. For this parametric experiment, the (3,3,2) hierarchical model was used because its convergence to the 3-D elasticity was verified through the previous verification experiment.

Figure 6a,b represent the calibrated fundamental frequencies versus the thickness-to-width ratios of (2-2-1) and (6-6-1) FG sandwich plates with homogeneous softcores. The bottom curve of the metal is the case of $n = 0$, while the top curve of the ceramic corresponds to $n = +\infty$. It was observed that the fundamental frequency increased in proportion to the volume fraction index, n . Referring to Figure 2, the relative amount of ceramic present in the plate increased in proportion to the volume fraction index, n . Furthermore, the ceramic was much stiffer than the metal, even though its density was greater than the metal's, as given in Table 1. For this reason, the sandwich plate became stiffer with the increasing value of the volume fraction index, n . Meanwhile, from Figure 6b, it may be seen that the frequencies of the center five curves became lower. This is because the relative amount of ceramic became smaller as the pseudo thickness ratio was changed from (2-2-1) to (6-6-1). In other words, the relative thickness ratio of metal core increased from 2/5 (= 40%) to 6/13 (= 46%).

Figure 7a,b represent the curves of FG sandwich plates with homogeneous hardcores. Because the core was ceramic, the bottom and top curves correspond to $n = +\infty$ and $n = 0$, respectively. Contrary to the previous softcore, the fundamental frequency decreased in proportion to the volume fraction index, n . This is because the sandwich plate with a hardcore became softer with the increasing value of the volume fraction index, n . The reason for this can be explained in the opposite manner to the previous softcore. Meanwhile, from Figure 7b, one can see that the frequencies of five curves in the middle became higher. This is because the relative amount of ceramic became larger as the pseudo thickness ratio was changed from (2-2-1) to (6-6-1).

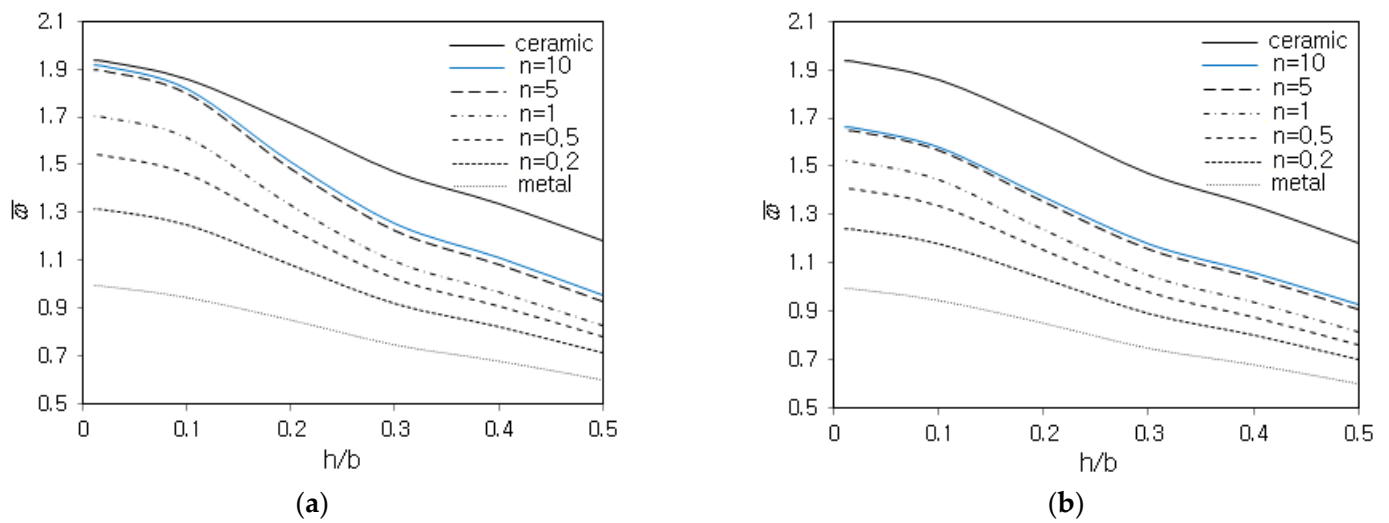


Figure 6. Calibrated fundamental frequencies, $\bar{\omega}$, for functionally graded sandwich plates with homogeneous softcores: (a) (2-2-1), (b) (6-6-1).

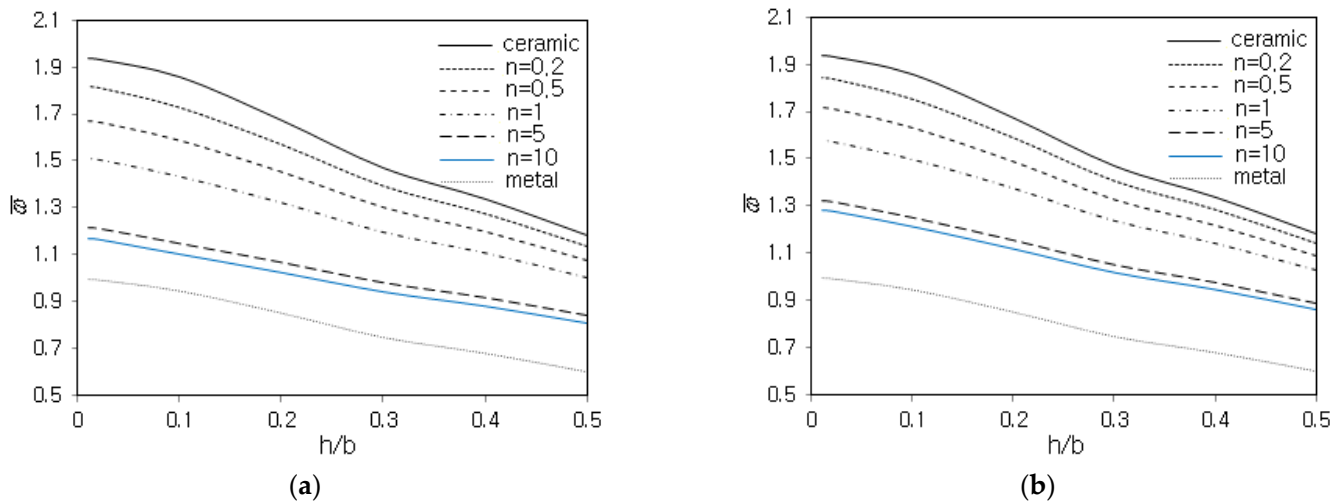


Figure 7. Calibrated fundamental frequencies, $\bar{\omega}$, for functionally graded sandwich plates with homogeneous hardcores: (a) (2-2-1), (b) (6-6-1).

Figure 8a,b represent the calibrated fundamental frequencies versus the volume fraction index, n , for (2-2-1) FG sandwich plates with homogenous cores. It is seen that the curves converged to the limits, both the fundamental frequencies of ceramic plates for softcore cases and those of metal plates for hardcore cases. The curves were upper-bounded for the softcore cases while those of the hardcore cases are lower-bounded. This limit characteristic, due to the material gradient in the FGM layers, could be confirmed from Figures 6a and 7a. With the increasing value of volume fraction index, n , two FGM layers in the softcore sandwich plate became ceramic-rich, while those in the hardcore sandwich plate became metal-rich. This fact can be confirmed from the volume fraction distributions shown in Figure 2. However, in both softcore and hardcore cases, it was observed that the calibrated fundamental frequency increased in proportion to the width-to-thickness ratio, b/h .

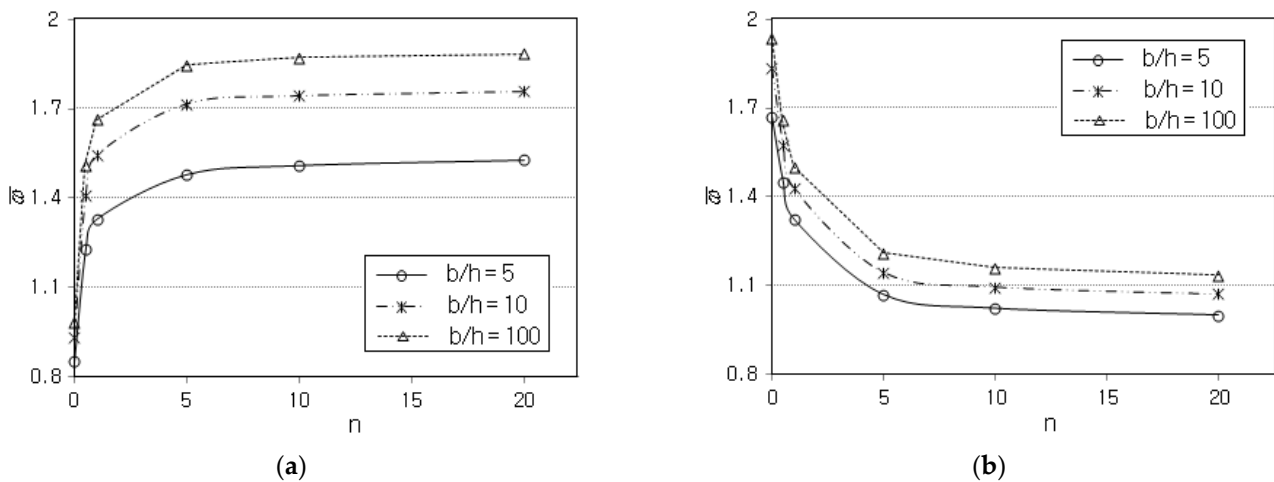


Figure 8. The gradient limits of calibrated fundamental frequency, $\bar{\omega}$, to the volume fraction index, n for: (a) softcore cases, (b) hardcore cases.

Tables 5 and 6 present the calibrated fundamental frequencies versus the relative thickness $R_3 = H_3 / (H_1 + H_2 + H_3)$ of the top facesheet of softcore and hardcore FG sandwich plates, respectively. The 8-8-1 and 16-16-1 configurations were included to examine the limits of $\bar{\omega}$ as R_3 tends to zero. The width-to-thickness ratio, b/h , of the sandwich plates was set by 10. The results are comparatively represented in Figure 9a,b, where the value, $\bar{\omega}$, of the $Al-Al_2O_3$ bi-material plate is 1.259. The curves of the softcore cases were lower-bounded because the amount of Ni slightly increased as R_3 became smaller. Conversely, those of hardcore cases were upper-bounded as R_3 became smaller, because the slight increase of the amount of Al_2O_3 . However, in both softcore and hardcore cases, the calibrated fundamental frequencies tended to 1.259 of $Al-Al_2O_3$ bi-material plate as the volume fraction index n tend to $+\infty$. This is because the $H_1 - H_2 - H_3 (H_1 = H_2)$ of the FG sandwich plates approached that of the $Al-Al_2O_3$ bi-material plates as H_1 and n tended to $+\infty$, regardless of the material type of core layer.

Table 5. The facesheet limits of the calibrated fundamental frequencies, $\bar{\omega}$, for simply supported square FG sandwich plates with homogeneous softcores ($b/h = 10$).

n	Softcore					
	1-1-1	2-2-1	3-3-1	4-4-1	8-8-1	16-16-1
0	0.93464	0.93464	0.93464	0.93464	0.93464	0.93464
0.5	1.45678	1.41018	1.37057	1.34075	1.27588	1.23348
1	1.60105	1.54583	1.49576	1.45646	1.36884	1.30447
5	1.77674	1.71733	1.65475	1.60164	1.47473	1.38047
10	1.80162	1.74416	1.67827	1.62098	1.48510	1.38334

Table 6. The facesheet limits of the calibrated fundamental frequencies, $\bar{\omega}$, for simply supported square FG sandwich plates with homogeneous hardcore ($b/h = 10$).

n	Hardcore					
	1-1-1	2-2-1	3-3-1	4-4-1	8-8-1	16-16-1
0	1.85670	1.85670	1.85670	1.85670	1.85670	1.85670
0.5	1.54887	1.58688	1.59295	1.60389	1.62626	1.63537
1	1.38588	1.43531	1.45256	1.46875	1.49820	1.52534
5	1.08127	1.14988	1.18662	1.21352	1.25575	1.28786
10	1.03080	1.10044	1.14199	1.17248	1.21105	1.25421

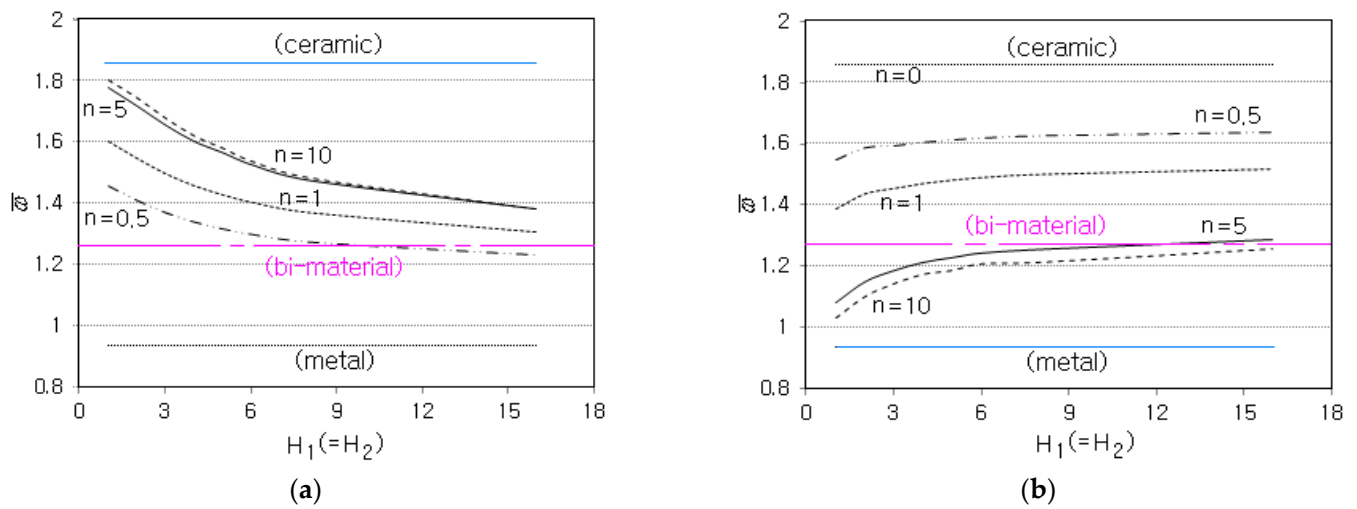


Figure 9. Variation of the calibrated fundamental frequency, $\bar{\omega}$, to the thickness, $H_1 (= H_2)$, of layers 1 and 2 for: (a) softcore cases; (b) hardcore cases.

Table 7 presents the calibrated fundamental frequencies, $\bar{\omega}$, of simply supported FG sandwich plates with respect to the aspect ratio a/b for various values of $R_3 = H_3 / (H_1 + H_2 + H_3)$. The volume fraction index, n , and the width-to-thickness ratio, b/h , were set at 1.0 and 10, respectively. The aspect ratio, a/b , was variable; changes to a were applied, while b was kept unchanged because the fundamental frequency was calibrated with respect to b , as given in Equation (22). It was found that the calibrated fundamental frequency increased, reversely proportional to the aspect ratio, regardless of the type of core, because the plate became stiffer as the aspect ratio decreased. This effect of the aspect ratio on the calibrated fundamental frequency is well represented in Figure 10a,b. Meanwhile, both softcore and hardcore cases show variations to the thickness, $H_1 (= H_2)$, which are similar to Figure 9a,b, respectively, regardless of the value of the aspect ratio.

Table 7. The effect of aspect ratio on the calibrated fundamental frequencies, $\bar{\omega}$, for simply supported FG sandwich plates with homogeneous cores ($n = 1, b/h = 10$).

a/b	$H_1-H_2-H_3$					
	1-1-1	2-2-1	3-3-1	4-4-1	8-8-1	16-16-1
	Softcore					
1	1.60105	1.54583	1.49576	1.45646	1.36884	1.30447
0.8	2.01452	1.94875	1.88814	1.83984	1.73081	1.65110
0.6	2.87617	2.78392	2.70324	2.63834	2.49003	2.38025
0.4	4.70632	4.59038	4.53748	4.50635	4.45577	4.30833
	Hardcore					
1	1.38588	1.43531	1.45256	1.46875	1.49820	1.52534
0.8	1.76225	1.81436	1.84618	1.86672	1.90385	1.92563
0.6	2.56688	2.64136	2.68659	2.71576	2.76846	2.79936
0.4	4.76499	4.89651	4.97526	5.02593	5.11735	5.17093

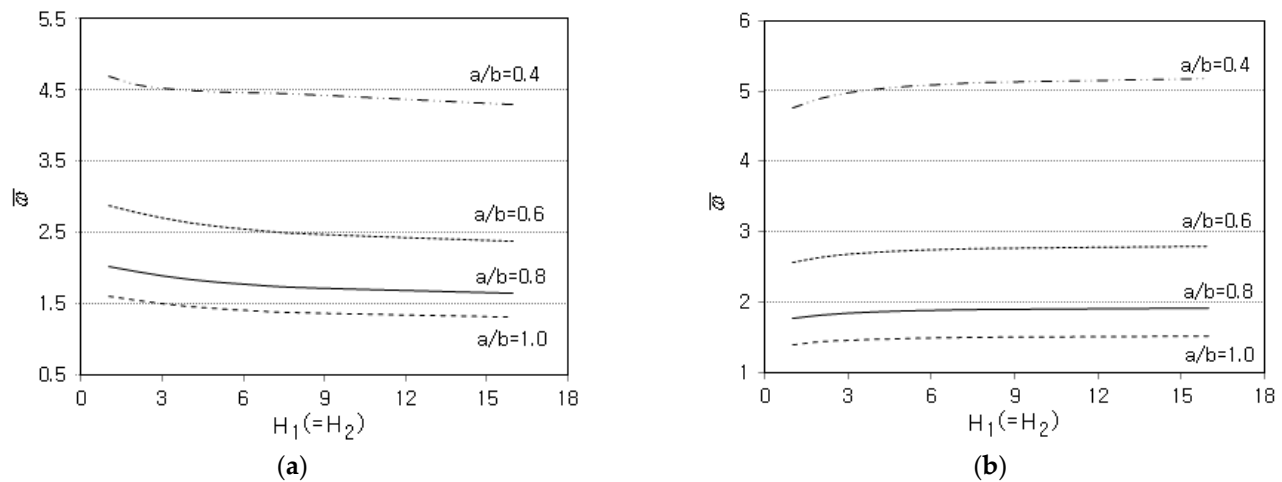


Figure 10. Effect of aspect ratio, a/b , on the calibrated fundamental frequency, $\bar{\omega}$ for: (a) softcore cases; (b) hardcore cases.

5. Conclusions

In this paper, a numerical method for the free vibration analysis of FG sandwich plates with homogeneous cores has been developed, using hierarchical models and the 2-D natural element method. The reliability of the proposed method was examined through the comparison with the reference and the 3-D elasticity. Furthermore, the free vibration characteristics of FG sandwich plates were parametrically investigated using the developed numerical method. Through the verification and parametric experiments, the following major observations were drawn:

- With respect to the 3-D elasticity, the relative differences in the calibrated fundamental frequencies of hierarchical models monotonically decreased with the increase of the model level, q . Meanwhile, the relative differences between the hierarchical models uniformly decreased as the plate thickness, h , became smaller.
- From the comparison with the reference, using the (1,1,0) hierarchical model, the present method showed a reasonable agreement with the maximum relative error of 7.961%. Meanwhile, the softcore and the hardcore showed a similar trend in the relative errors with respect to n , but both cores exhibited the contrary trend with respect to b/h .
- In the FG sandwich plates with softcores, the calibrated fundamental frequencies increased in proportion to the volume fraction index, n , and in reverse proportions to the plate aspect ratio. Furthermore, the frequency curves became lower as the pseudo thickness ratio was changed from (2-2-1) to (6-6-1). However, these trends became entirely reversed for the plates with hardcores.
- In (2-2-1) FG sandwich plates with softcores, the calibrated fundamental frequencies were lower-bounded with respect to the thickness of the top facesheet. However, the frequency curves were upper-bounded for the plates with hardcores. Both cases commonly approach the $Al-Al_2O_3$ bi-material plate as H_1 and n tend to $+\infty$.

Funding: This work was supported by a National Research Foundation of Korea (NRF) grant funded by the Korean government (MSIT) (2020R1A2C1100924).

Conflicts of Interest: The author declares no conflict of interest.

References

1. Cho, J.R.; Oden, J.T. Functionally graded material: A parametric study on thermal-stress characteristics using the Crank-Nicolson-Galerkin scheme. *Comput. Methods Appl. Mech. Eng.* **2000**, *188*, 17–38. [\[CrossRef\]](#)
2. Miyamoto, Y.; Kaysser, W.W.; Rabin, B.H.; Kawasaki, A.; Ford, R.G. *Functionally Graded Materials: Design, Processing and Applications*; Springer Science+ Business Media: New York, NY, USA, 1999.

3. Zenkour, A.M. A comprehensive analysis of functionally graded sandwich plates: Part 1—Deflection and stresses. *Int. J. Solids Struct.* **2005**, *42*, 5224–5242. [[CrossRef](#)]
4. Cho, J.R.; Ha, D.Y. Volume fraction optimization for minimizing thermal stress in Ni-Al₂O₃ functionally graded materials. *Mater. Sci. Eng. A* **2002**, *334*, 147–155. [[CrossRef](#)]
5. Nie, G.J.; Zhong, Z.; Batra, R.C. Material tailoring for reducing stress concentration factor at a circular hole in a functionally graded materials (FGM) panel. *Compos. Struct.* **2018**, *205*, 49–57. [[CrossRef](#)]
6. Chmielewski, M.; Pietrzak, K. Metal-ceramic functionally graded materials—Manufacturing, characterization, application. *Bull. Pol. Acad. Sci.* **2016**, *64*, 151–160. [[CrossRef](#)]
7. Kashtalyan, M.; Menshykova, M. Three-dimensional elasticity solution for sandwich panels with a functionally graded core. *Compos. Struct.* **2009**, *87*, 36–43. [[CrossRef](#)]
8. Li, D.; Deng, Z.; Xiao, H.; Jin, P. Bending analysis of sandwich plates with different face sheet materials and functionally graded soft core. *Thin-Walled Struct.* **2018**, *122*, 8–16. [[CrossRef](#)]
9. Das, M.; Barut, B.; Madenci, E.; Ambur, D.R. A triangular plate element for thermo-elastic analysis of sandwich panels with a functionally graded core. *Int. J. Numer. Methods Eng.* **2006**, *68*, 940–966. [[CrossRef](#)]
10. Bennoun, M.; Houari, M.S.A.; Tounsi, A. A novel five-variable refined plate theory for vibration analysis of functionally graded sandwich plates. *Mech. Mater. Struct.* **2016**, *23*, 423–431. [[CrossRef](#)]
11. Li, Q.; Lu, V.P.; Kou, K.P. Three-dimensional vibration analysis of functionally graded material sandwich plates. *J. Sound Vib.* **2008**, *311*, 498–515. [[CrossRef](#)]
12. Zenkour, A.M. A comprehensive analysis of functionally graded sandwich plates: Part 2—Buckling and free vibration. *Int. J. Solids Struct.* **2005**, *42*, 5243–5258. [[CrossRef](#)]
13. Yaghoobi, H.; Yaghoobi, P. Buckling analysis of sandwich plates with FGM face sheets resting on elastic foundation with various boundary conditions: An analytical approach. *Meccanica* **2013**, *48*, 2019–2035. [[CrossRef](#)]
14. Hadji, L.; Atmane, H.A.; Tounsi, A.; Mechab, I.; Adda Bedia, E.A. Free vibration of functionally graded sandwich plates using four variable refined plate theory. *Appl. Math. Mech.* **2011**, *32*, 925–942. [[CrossRef](#)]
15. El Meiche, N.; Tounsi, A.; Ziane, N.; Mechab, I.; Adda Bedia, E.A. A new hyperbolic shear deformation theory for buckling and vibration of functionally graded sandwich plate. *Int. J. Mech. Sci.* **2011**, *53*, 237–247. [[CrossRef](#)]
16. Houari, M.S.A.; Benyoucef, S.; Mechab, I.; Tounsi, A.; Adda Bedia, E.A. Two variable refined plate theory for thermoelastic bending analysis of functionally graded sandwich plates. *J. Therm. Stress.* **2011**, *34*, 315–334. [[CrossRef](#)]
17. Carrera, E.; Brischetto, S.; Cinefra, M.; Soave, M. Effects of thickness stretching in functionally graded plates and shells. *Compos. Part B* **2011**, *42*, 123–133. [[CrossRef](#)]
18. Pandey, S.; Pradyumna, S. Free vibration of functionally graded sandwich plates in thermal environment using a layerwise theory. *Euro. J. Mech. A/Solids* **2015**, *15*, 55–66. [[CrossRef](#)]
19. Xiang, S.; Kang, G.; Yang, M.; Zhao, Y. Natural frequencies of sandwich plate with functionally graded face and homogeneous core. *Compos. Struct.* **2013**, *96*, 226–231. [[CrossRef](#)]
20. Di Sciuva, M.; Sorrenti, M. Bending and free vibration analysis of functionally graded sandwich plates: An assessment of the Refined Zigzag Theory. *J. Sandwich Struct. Mater.* **2019**, *23*, 760–802. [[CrossRef](#)]
21. Liu, J.; Hao, C.; Yang, W.; Lin, G. Free vibration and transient dynamic response of functionally graded sandwich plates with power-law nonhomogeneity by the scaled boundary finite element method. *Comput. Methods Appl. Mech. Eng.* **2021**, *376*, 113665. [[CrossRef](#)]
22. Vinh, P.V. Analysis of bi-directional functionally graded sandwich plates via higher-order shear deformation theory and finite element method. *J. Sandwich Struct. Mater.* **2022**, *24*, 860–899. [[CrossRef](#)]
23. Vinh, P.V. Deflections, stresses and free vibration analysis of bi-functionally graded sandwich plates resting on Pasternak’s elastic foundations via hybrid quasi-3D theory. *Mech. Based Des. Struct. Mach.* **2021**, *in press*.
24. Vinh, P.V.; Huy, L.Q. Finite element analysis of functionally graded sandwich plates with porosity via a new hyperbolic shear deformation theory. *Def. Technol.* **2022**, *18*, 490–508. [[CrossRef](#)]
25. Hirane, H.; Belarbi, M.O.; Houari, M.S.A.; Tounsi, A. On the layerwise finite element formulation for static and free vibration analysis of functionally graded sandwich plates. *Eng. Comput.* **2021**, *in press*. [[CrossRef](#)]
26. Belarbi, M.O.; Li, L.; Houari, M.S.A.; Garg, A.; Chalak, H.D.; Dimitri, R.; Tornabene, F. Nonlocal vibration of functionally graded nanoplates using a layerwise theory. *Math. Mech. Solids* **2022**, *in press*. [[CrossRef](#)]
27. Vinh, P.V.; Tounsi, A. The role of spatial variation of the nonlocal parameter on the free vibration of functionally graded sandwich nanoplates. *Eng. Struct.* **2021**, *in press*. [[CrossRef](#)]
28. Cho, J.R. Natural element approximation of hierarchical models of plate-like elastic structures. *Finite Elem. Anal. Des.* **2020**, *180*, 103439. [[CrossRef](#)]
29. Cho, J.R. Hierarchic models for the free vibration analysis of functionally graded plates. *Int. J. Mech. Mater. Des.* **2021**, *17*, 489–501. [[CrossRef](#)]
30. Sukumar, N.; Moran, B. C^1 natural neighbor interpolant for partial differential equations. *Numer. Methods Partial. Differ. Equ.* **1999**, *15*, 417–447. [[CrossRef](#)]
31. Cho, J.R.; Ha, D.Y. Averaging and finite-element discretization approaches in the numerical analysis of functionally graded materials. *Mater. Sci. Eng. A* **2001**, *302*, 187–196. [[CrossRef](#)]

32. Chinesta, F.; Cescotto, C.; Cueto, E.; Lorong, P. *Natural Element Method for the Simulation of Structures and Processes*; Wiley: Hoboken, NJ, USA, 2013.
33. Cho, J.R.; Lee, H.W. A Petrov-Galerkin natural element method securing the numerical integration accuracy. *J. Mech. Sci. Technol.* **2006**, *20*, 94–109. [[CrossRef](#)]
34. Zienkiewicz, O.C.; Taylor, R.L.; Too, J.M. Reduced integration technique in general analysis of plates and shells. *Int. J. Numer. Methods Eng.* **1971**, *3*, 275–290. [[CrossRef](#)]
35. ANSYS. *Users Guide for Release 20.0, Structural Analysis Guide*; ANSYS: Canonsburg, PA, USA, 2020.
36. Reddy, J.N. *Mechanics of Laminated Plates and Shell Theory and Analysis*, 2nd ed.; CRC Press: New York, NY, USA, 2004.